[redacted]

Copy 6
RM L54H25

NACA RM L54H25

NACA

RESEARCH MEMORANDUM

A TRANSONIC WIND-TUNNEL INVESTIGATION OF THE LONGITUDINAL FORCE AND MOMENT CHARACTERISTICS OF A PLANE AND A CAMBERED 3-PERCENT-THICK DELTA WING OF ASPECT RATIO 3 ON A SLENDER BODY

By Dale L. Burrows and William E. Palmer

Langley Aeronautical Laboratory
Langley Field, Va.

NATIONAL ADVISORY COMMITTEE
FOR AERONAUTICS

WASHINGTON

November 15, 1954

[redacted]

NATIONAL ADVISORY COMMITTEE FOR AERONAUTICS

RESEARCH MEMORANDUM

A TRANSONIC WIND-TUNNEL INVESTIGATION OF THE LONGITUDINAL FORCE AND MOMENT CHARACTERISTICS OF A PLANE AND A CAMBERED 3-PERCENT-THICK DELTA WING OF ASPECT RATIO 3 ON A SLENDER BODY

By Dale L. Burrows and William E. Palmer

SUMMARY

Various investigations have indicated the usefulness of some form of leading-edge droop on thin, swept-wing designs in reducing drag due to lift; notably, the droop has usually amounted to some combination of camber and twist. In the present investigation, the effects of leading-edge camber without twist were determined on an aspect-ratio-3 delta wing of thickness ratio 3 in combination with a body having an ogive nose and a cylindrical afterbody. The investigation covered a Mach number range from 0.67 to 1.38 and the Reynolds numbers were about 5.5×10^6 up to an angle of attack of 12° and about 2.7×10^6 at angles of attack from 10° to 20°.

Drag of the cambered wing at lifting conditions was reduced over that of the plane wing with the result that maximum lift-drag ratios were increased about 5 percent over the range of Mach numbers from 0.76 to 1.2. This improvement due to camber diminished appreciably at higher Mach numbers. The lift-curve slope for the cambered wing was essentially the same as that for the plane wing throughout the test range of Mach numbers. The leading-edge camber considerably reduced the large variations in longitudinal stability experienced by the plane wing at lift coefficients of about 0.5 at high subsonic Mach numbers.

INTRODUCTION

The reduction of drag on thin swept wings at lifting conditions and at transonic speeds would appear to involve the solution of two problems. First, in order to minimize the drag resulting from induced flows, Jones has shown that the lift should be distributed over the surface such that

the spanwise and chordwise load distributions are elliptical (ref. 1). Second, the surface-pressure distribution over the leading edge should be free of pressure gradients sufficiently steep to cause boundary-layer separation and, hence, loss of leading-edge suction. At lifting conditions, both of these requirements imply the use of camber and twist to obtain overall drag reduction even though the zero-lift drag may be increased. A wing which was cambered and twisted conically over the outboard twenty percent of the local semispan in such a way as to give nearly an elliptical span-load distribution produced some drag improvements at lifting conditions and at high subsonic Mach numbers as shown in reference 2. Another case of camber and twist in the form of a constant-chord leading-edge droop was found to give comparable drag reductions at high subsonic speeds (ref. 3).

The purpose of the present investigation was to determine whether leading-edge camber (without twist) on a delta wing would produce drag improvements at lifting conditions over the drag of the flat wing at transonic speeds. The wing contour was obtained by drooping the leading 25 percent of the chord of all streamwise airfoil sections. The investigation consisted of experimental measurements of the lift, drag, and pitching moment on the cambered wing and a flat wing of the same plan form. The wings had delta plan forms, had an aspect ratio of 3.0, and were 3 percent thick. The tests were made at Mach numbers from 0.67 to 1.38 and the Reynolds numbers, based on the mean aerodynamic chord, were about 5.5×10^6 up to an angle of attack of 12° and about 2.7×10^6 at angles of attack from 10° to 20°.

SYMBOLS

C_D	drag coefficient, $\frac{\text{Drag}}{qS}$
C_{D_o}	zero-lift drag coefficient, $\frac{\text{Drag}}{qS}$
C_L	lift coefficient, $\frac{\text{Lift}}{qS}$
C_m	pitching-moment coefficient, $\frac{\text{Pitching moment about } \bar{c}/4}{qS\bar{c}}$
L/D	lift-drag ratio
$(L/D)_{max}$	maximum value of lift-drag ratio
$C_{L_{opt}}$	lift coefficient at $(L/D)_{max}$

A	aspect ratio
b	total wing span
$\bar{c}$	wing mean aerodyanmic chord, $\frac{2}{S}\int_0^{b/2} c^2\,dy$
c	wing chord at any value of y
K	coefficient of drag due to lift, $\frac{C_D - C_{D_o}}{C_L^2}$
M	average free-stream Mach number at model location
M_x	local free-stream Mach number at model location
p_b	static pressure inside open base of model
p	free-stream static pressure
P_s	free-stream absolute stagnation pressure
q	free-stream dynamic pressure, $\frac{\gamma p M^2}{2}$
γ	ratio of specific heats, 1.40 for air
R	free-stream Reynolds number based on $\bar{c}$
S	total wing area
y	spanwise distance from and normal to model center line
α	angle of attack of the fuselage center line, deg

APPARATUS AND METHODS

Tunnel

The tests were conducted in the Langley transonic blowdown tunnel which has a slotted octagonal test section and exhausts to atmosphere from total stagnation pressures that can be adjusted to values as high as 72 pounds per square inch absolute. Dried air is used to operate the blowdown tunnel. At a stagnation pressure of 70 pounds per square inch absolute, the tunnel running time is about 20 seconds. Mach numbers up

[redacted]

to approximately 1.4 can be attained and, at a given Mach number, the Reynolds number can be varied from approximately 8×10^6 per foot of chord to 24×10^6 per foot of chord by varying the stagnation pressure from 25 pounds per square inch absolute to 70 pounds per square inch absolute. The Mach number distribution along that part of the tunnel center line where the model was located is shown in figure 1. The angle-of-attack mechanism was such as to keep the model centrally located in the tunnel throughout the angle-of-attack range.

Models

Details of the models are shown in figure 2. The wings were made of solid steel and had 45° sweepback of the quarter-chord line, a zero taper ratio, and an aspect ratio 3. The uncambered wing had NACA 65A003 airfoil sections parallel to the plane of symmetry and the cambered wing had the same thickness ordinates distributed about a mean line having two-thirds the ordinates of an NACA 230 mean line (see table I). The resultant design lift coefficient was 0.2 and the airfoil is designated NACA 65A203 (230 modified). The wings were mounted with zero incidence and zero dihedral on the body.

The body with a fineness ratio of 9.63 was a hollow steel shell having an ogive nose 3.5 diameters in length and a cylindrical afterbody. Housed within the body was a three-component electrical strain-gage balance which was attached to a sting for support of the model. The sting was of constant diameter for 1.75 body diameters back of the base of the model after which it diverged at a cone angle of 9.7° (fig. 2). Two tubes for measuring base pressures were attached to the sides of the sting and extended into the open annulus at the model base. Photographs of the model are shown as figure 3.

Tests

The investigation covered a Mach number range from 0.67 to 1.30 at angles of attack from 0° to 12° for a stagnation pressure of 70 pounds per square inch absolute and at 10° to 20° for a pressure of 35 pounds per square inch absolute. For a Mach number of 1.38, data were obtained at a pressure of 50 pounds per square inch absolute up to an angle of attack of 12°. These limits of angle of attack and stagnation pressure were dictated by the balance load limits. Body-alone data were obtained at angles of attack up to 6°. The Reynolds numbers based on $\bar{c}$ for the various stagnation pressures are shown in figure 4. For all tests, the surface of the model was in a smooth condition. Shock reflection from the tunnel wall intersected the model at Mach numbers between about 1.04 and 1.10; carry-over effects through the boundary layer may extend this range to a slightly higher Mach number. This condition may introduce

appreciable tunnel effects on the force and moment data and, therefore, such data are not presented for this Mach number range.

Measurements and Accuracy

Normal-force, chord-force, pitching-moment, and base-pressure data were recorded simultaneously on film. The chord-force coefficient, which included the pressure force on the model base, was adjusted to a condition of base pressure equal to free-stream static pressure. Normal- and chord-force coefficients were converted to lift and drag coefficients by the usual methods. On the basis of the balance sensitivity, scatter of test points, and repeatability of data, at low angles of attack the estimated accuracy of lift, drag, and pitching-moment coefficients is ±0.02, ±0.001, and ±0.003, respectively. Mach numbers shown with the data are accurate to about ±0.01.

Corrections

Reference 4 shows that, for slotted tunnels, where the ratio of model size to test-section size is about equal to that of the present investigation, the jet-boundary effects are negligible; therefore, no such correction has been made to the data. Angle of attack was corrected for sting deflection resulting from aerodynamic load.

An investigation was made of the static elastic bending and twisting of the plane wing under simulated maximum load. Results indicated that, for the maximum load condition ($M = 1.30$, $P_s = 70$ pounds per square inch absolute), aeroelasticity produced a decrease in lift-curve slope on the order of 2 percent and a forward shift in aerodynamic-center position of about $0.01\bar{c}$. In the data presented, however, no correction for aeroelasticity has been applied.

PRESENTATION OF RESULTS

The results of this investigation are presented in the following figures:

	Figure
$\frac{p_b - p_o}{q}$ against M	5
C_L, C_D, and C_m against α for body alone	6
C_L, C_D, and C_m against M for body alone	7
C_L against α for plane wing	8(a)
C_L against α for cambered wing	8(b)
$(dC_L/d\alpha)_{C_L=0}$ against M for both wings	9

DISCUSSION

Base Pressures and Body Characteristics

The increment in base-pressure coefficient between body-alone and wing-body combinations (fig. 5) is about the same as that shown in references 5 and 6 and indicates that the effect is relatively independent of wing plan form. Figure 5 shows also that there is no appreciable difference between the base pressures for the flat wing and those for the cambered wing investigated. The large irregularities in the variation of base-pressure coefficient with Mach number that occurred at low supersonic speeds are due to the wall-reflected shock waves mentioned previously.

The lift, drag, and pitching-moment characteristics of the body alone (fig. 6) are essentially the same as for body "C" of reference 5; this would be expected because of the similarity of body shapes. Figure 7 shows little variation of lift and pitching-moment coefficients with Mach number for angles of attack up to 6°.

Wing-Body Combinations

Lift characteristics.- As shown in figure 8, the plane and the cambered wings exhibit generally similar lift characteristics except for a "jog" in the variation of lift coefficient with angle of attack at a Mach number of 0.96 and a lift coefficient of about 0.7 that occurs only for the plane wing. As shown in figure 9, the values of $(dC_L/d\alpha)_{C_L=0}$ are essentially the same for the cambered wing as for the plane wing over the test Mach number range. The method of reference 7 has been used to determine the theoretical lift-curve slopes of the wing-body combination. This method required wing-alone lift-curve slopes which were obtained from the theories of DeYoung (ref. 8) and Brown (ref. 9), respectively, for the subsonic and supersonic speed range. Experimental values of

lift-curve slope are as much as 12 percent lower than those given by theory and the variation with Mach number at Mach numbers near unity is much less pronounced than that given by theory.

Drag characteristics.- Basic drag data are plotted against C_L in figures 10(a) and 10(b). Figure 11 shows that values of drag coefficient are generally slightly higher for the cambered wing than for the plane wing at Mach numbers greater than 0.85 and lift coefficients of 0.0 and 0.1. At lift coefficients greater than 0.2, the drag coefficient is lower for the cambered wing at all test Mach numbers. At zero lift the rise in drag coefficient through the transonic Mach number range was about 0.007 for both wing-body combinations.

Values of $(L/D)_{max}$ and $C_{L_{opt}}$ taken from figure 12 are presented in figure 13 and show an increase in $(L/D)_{max}$ due to camber of approximately 5 percent at Mach numbers up to about 1.20. This benefit due to camber was essentially lost at a Mach number of 1.38. From a comparison of this benefit with the 20-percent increase at subsonic speeds and the 10-percent increase at low supersonic speeds resulting from the conical camber and twist of reference 2, it would seem that the leading-edge camber reported herein was inferior to the conical camber and twist; a direct comparison of the two types of delta wings, however, is not justified, inasmuch as the aspect ratio was 2 for the conical camber and twisted wing as compared with an aspect ratio of 3 for the leading-edge cambered wing. The gradual reduction in effectiveness of camber alone with increasing Mach number is in agreement with the conclusion of reference 2 which indicates that the benefits of camber and twist are considerably reduced when the component of free-stream Mach number perpendicular to the wing leading edge becomes approximately 0.7. This conclusion seems reasonable when one considers that the leading-edge suction in both cases rapidly disappears as the Mach cone approaches the leading edge.

The theoretical values of $(L/D)_{max}$ shown in figure 13 were obtained for the flat wing without consideration of body effects according to the expression $\frac{1}{2}\sqrt{\frac{1}{KC_{D_o}}}$ where C_{D_o} values were taken from plane-wing data. For the full leading-edge suction case, K was taken as $\frac{1}{\pi A}$ at subsonic speeds and at supersonic speeds the method of reference 9 was used. For zero leading-edge suction, the value of K was taken as $\frac{1}{57.3\left(\frac{dC_L}{d\alpha}\right)_{C_L=0}}$ where values of $\left(\frac{dC_L}{d\alpha}\right)_{C_L=0}$ were theoretical values obtained for the plane wing. In general, the measured values of $(L/D)_{max}$ fall between

[redacted]

the theoretical limits as would be expected; however, the closer approach to full leading-edge suction at the higher Mach numbers is contrary to the usual assumption of zero leading-edge suction as the Mach cone approaches the leading edge.

Pitching-moment characteristics.- A break occurs in the curve of C_m against C_L for the plane wing (fig. 14(a)) at a lift coefficient of 0.5 and a Mach number of 0.76. As the Mach number is increased to 0.96, this change in longitudinal stability becomes more severe and occurs at a higher lift coefficient. No such break is present at supersonic Mach numbers. There is some indication that the flow on the plane wing may be affected by Reynolds number. (See the curve for $M = 0.96$.) Figure 14(b) shows that for the cambered wing the stability break is eliminated at all Mach numbers except near 0.96 where the break is much less severe than for the plane wing.

The camber produced a change in pitching-moment coefficient at zero lift which is small but in a direction to require more elevator deflection for trim (fig. 14(b)); this effect comes about because the chord line was alined with the fuselage. In general, for higher lifts, values of C_m are more negative for the cambered wing at lift coefficients up to 0.6 (fig. 15); this result does not seem unlikely when it is considered that the separation on the plane-wing leading edge is small as evidenced by fairly high leading-edge suction in which case the usual effect of camber is to produce a rearward shift in center of pressure. At lift coefficients of 0.2 to 0.6, figure 15 shows that an abrupt increase in negative pitching-moment coefficient (rearward movement in center of pressure) occurs for both wings at a Mach number of about 0.93. Although the total increase in moment coefficient with Mach number is about the same for the two wings, the change with Mach number is more gradual for the cambered wing than for the plane wing.

It is seen from figure 16 that there is no appreciable difference between the aerodynamic-center locations (dC_m/dC_L at zero lift) for the two wings. Subsonically, C_m varies almost linearly with C_L only up to lift coefficients of 0.4 to 0.5. Trends with Mach number agree with theory, but theoretical values of the aerodynamic center are on the order of $0.025\bar{c}$ rearward of the experimental values. For determination of the theoretical values of aerodynamic center for the wing-body combination, the method of reference 7 has been used. This method required the wing-alone lift-curve slopes, which were obtained from references 8 and 9, and the wing-alone centers of pressure, which were obtained from reference 10.

CONCLUSIONS

Tests at transonic speeds of 3-percent-thick, aspect-ratio-3, delta-wing-fuselage configurations both with and without leading-edge camber resulted in the following conclusions:

1. This type of camber produced an increase in maximum lift-drag ratio of about 5 percent for Mach numbers from 0.76 to 1.20. The benefit diminished at Mach numbers of 1.20 to 1.38.

2. The cambered wing had lower drag coefficients at values of lift coefficient greater than about 0.2 at all Mach numbers tested.

3. Drag-coefficient rise through the transonic speed range for both wing-fuselage combinations at zero lift was about 0.007.

4. The lift-curve slope for the cambered wing was essentially the same as that for the plane wing through the Mach number range tested.

5. The longitudinal static stability at zero lift was essentially the same for both plane and cambered wings throughout the Mach number range.

6. Irregularities in the longitudinal stability of the plane wing at moderate lift coefficients and high subsonic speeds were essentially eliminated by the use of the leading-edge camber investigated.

Langley Aeronautical Laboratory,
National Advisory Committee for Aeronautics,
Langley Field, Va., August 12, 1954.

[redacted]

1. Jones, Robert T.: The Minimum Drag of Thin Wings in Frictionless Flow. Preprint no. 289, S.M.F. Final Paper, Inst. Aero. Sci., July 1950.

2. Hall, Charles F.: Lift, Drag, and Pitching Moment of Low-Aspect-Ratio Wings at Subsonic and Supersonic Speeds. NACA RM A53A30, 1953.

3. Polhamus, Edward C.: Drag Due to Lift at Mach Numbers up to 2.0. NACA RM L53I22b, 1953.

4. Whitcomb, Charles F., and Osborne, Robert S.: An Experimental Investigation of Boundary Interference on Force and Moment Characteristics of Lifting Models in the Langley 16- and 8-Foot Transonic Tunnels. NACA RM L52L29, 1953.

5. Loving, Donald L., and Wornom, Dewey E.: Transonic Wind-Tunnel Investigation of the Interference Between a 45° Sweptback Wing and a Systematic Series of Four Bodies. NACA RM L52J01, 1952.

6. Estabrooks, Bruce B.: Transonic Wind-Tunnel Investigation of an Unswept Wing in Combination With a Systematic Series of Four Bodies. NACA RM L52K12a, 1953.

7. Nielson, Jack N., Kaattari, George E., and Anastasio, Robert F.: A Method of Calculating the Lift and Center of Pressure of Wing-Body-Tail Combinations at Subsonic, Transonic, and Supersonic Speeds. NACA RM A53G08, 1953.

8. DeYoung, John, and Harper, Charles W.: Theoretical Systematic Span Loading at Subsonic Speeds for Wings Having Arbitrary Plan Form. NACA Rep. 921, 1948.

9. Brown, Clinton E.: Theoretical Lift and Drag of Thin Triangular Wings at Supersonic Speeds. NACA Rep. 839, 1946. (Supersedes NACA TN 1183.)

10. Lomax, Harvard, and Sluder, Loma: Chordwise and Compressibility Corrections to Slender-Body Theory. NACA Rep. 1105, 1952. (Supersedes NACA TN 2295.)

[redacted]

TABLE I

COORDINATES OF AIRFOIL AND MEAN LINE PARALLEL TO PLANE OF SYMMETRY FOR BOTH A PLANE AND A CAMBERED DELTA WING WITH A THICKNESS RATIO OF 3 PERCENT AND AN ASPECT RATIO OF 3

[Stations, ordinates, and radii given in percent of airfoil chord.]

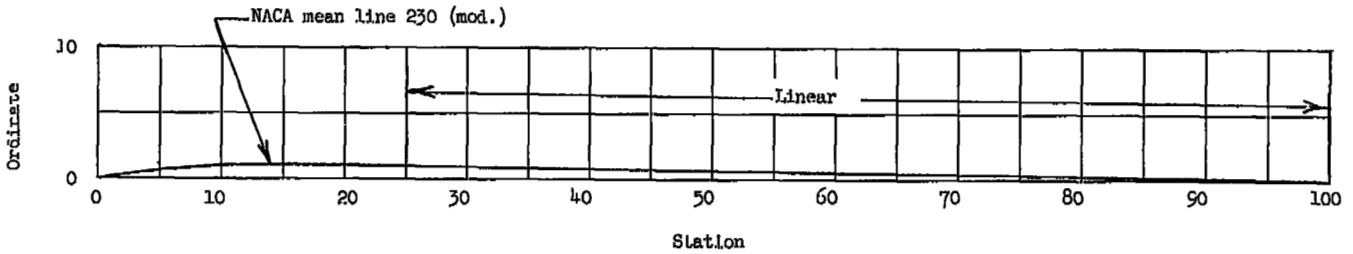

NACA 65A003			NACA 65A203 (230 mod.)				NACA mean line 230 (mod.)		
Station	Upper surface ordinate	Lower surface ordinate	Upper surface		Lower surface		Station	230 ordinate	230 (mod.) ordinate
			Station	Ordinate	Station	Ordinate			
0	0	0	0	0	0	0	0	0	0
1.25	.362	-.362	1.187	.594	1.313	-.118	1.25	.357	.238
2.5	.493	-.493	2.426	.931	2.574	-.043	2.5	.666	.444
5.0	.658	-.658	4.929	1.424	5.071	.116	5.0	1.155	.770
7.5	.796	-.796	7.443	1.789	7.557	.201	7.5	1.492	.995
10	.912	-.912	9.962	2.044	10.038	.224	10	1.701	1.134
15	1.097	-1.097	15.000	2.322	15.000	.128	15	1.838	1.225
20	1.236	-1.236	20.018	2.414	19.982	-.050	20	1.767	1.178
25	1.342	-1.342	25.020	2.446	24.980	-.238	25	1.656	1.104
30	1.420	-1.420	30.021	2.451	29.979	-.389	30	1.546	1.031
40	1.498	-1.498	40.022	2.381	39.978	-.615	40	1.325	.883
50	1.465	-1.465	50.022	2.201	49.978	-.729	50	1.104	.736
60	1.309	-1.309	60.019	1.898	59.981	-.720	60	.883	.589
70	1.053	-1.053	70.016	1.494	69.984	-.612	70	.662	.441
80	.727	-.727	80.011	1.022	79.989	-.432	80	.442	.295
90	.369	-.369	90.005	.516	89.995	-.222	90	.221	.147
95	.188	-.188	95.003	.261	94.997	-.115	95	.110	.073
100	.007	-.007	100.000	.007	100.000	-.007	100	0	0
L.E. radius: 0.057 T.E. radius: 0.0068			L.E. radius: 0.057 T.E. radius: 0.0068						

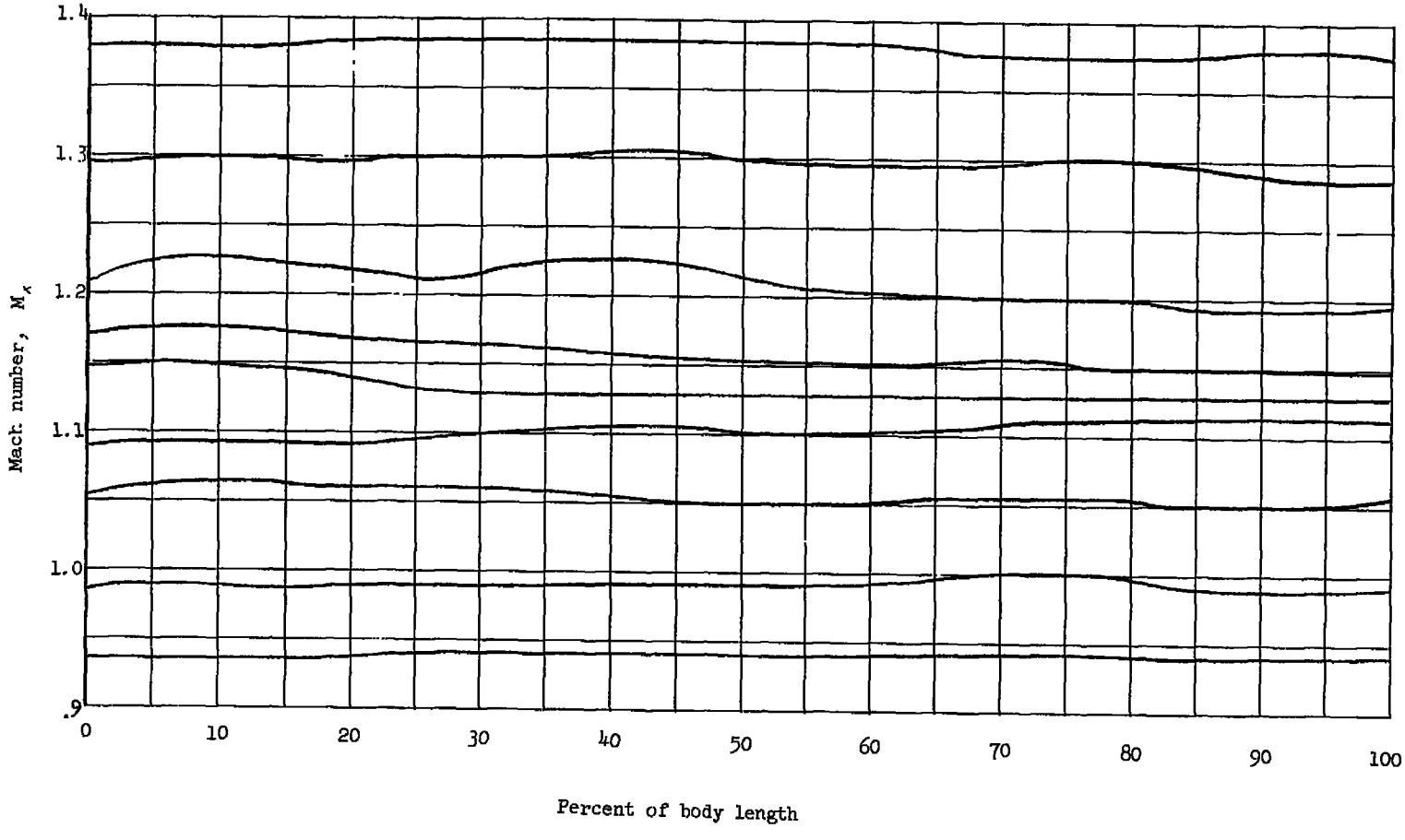

Figure 1.- Longitudinal free-stream Mach number distribution at the location of the model for several average Mach numbers.

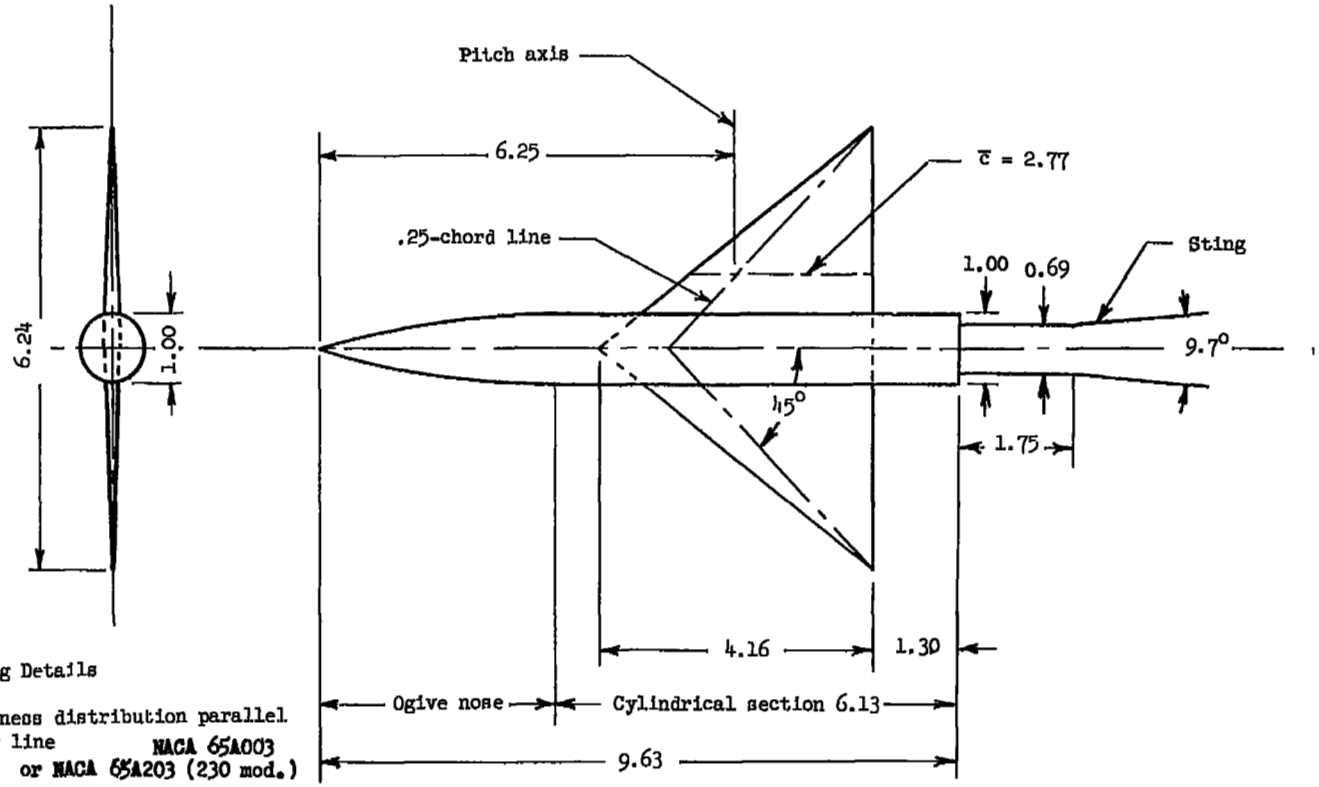

Wing Details

Basic airfoil thickness distribution parallel to model center line	NACA 65A003 or NACA 65A203 (230 mod.)
Area, sq. in.	12.96
Aspect ratio	3
Taper ratio	0
Sweepback of quarter-chord line, deg.	45
Incidence, deg.	0
Dihedral, deg.	0

Figure 2.- Details of the wing-body configurations. All dimensions are in inches.

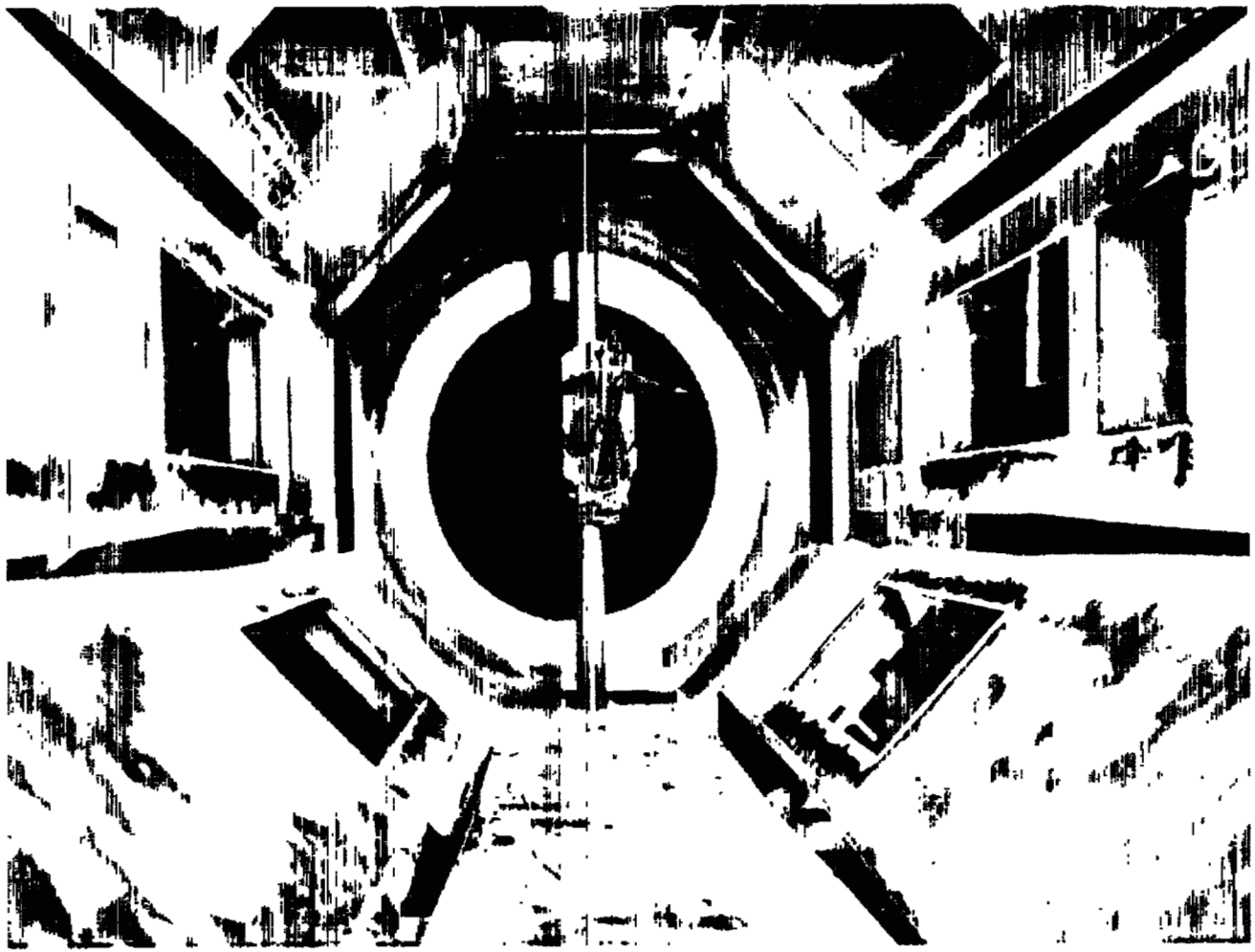

(a) Downstream view.

L-82449

Figure 3.- Photographs of model.

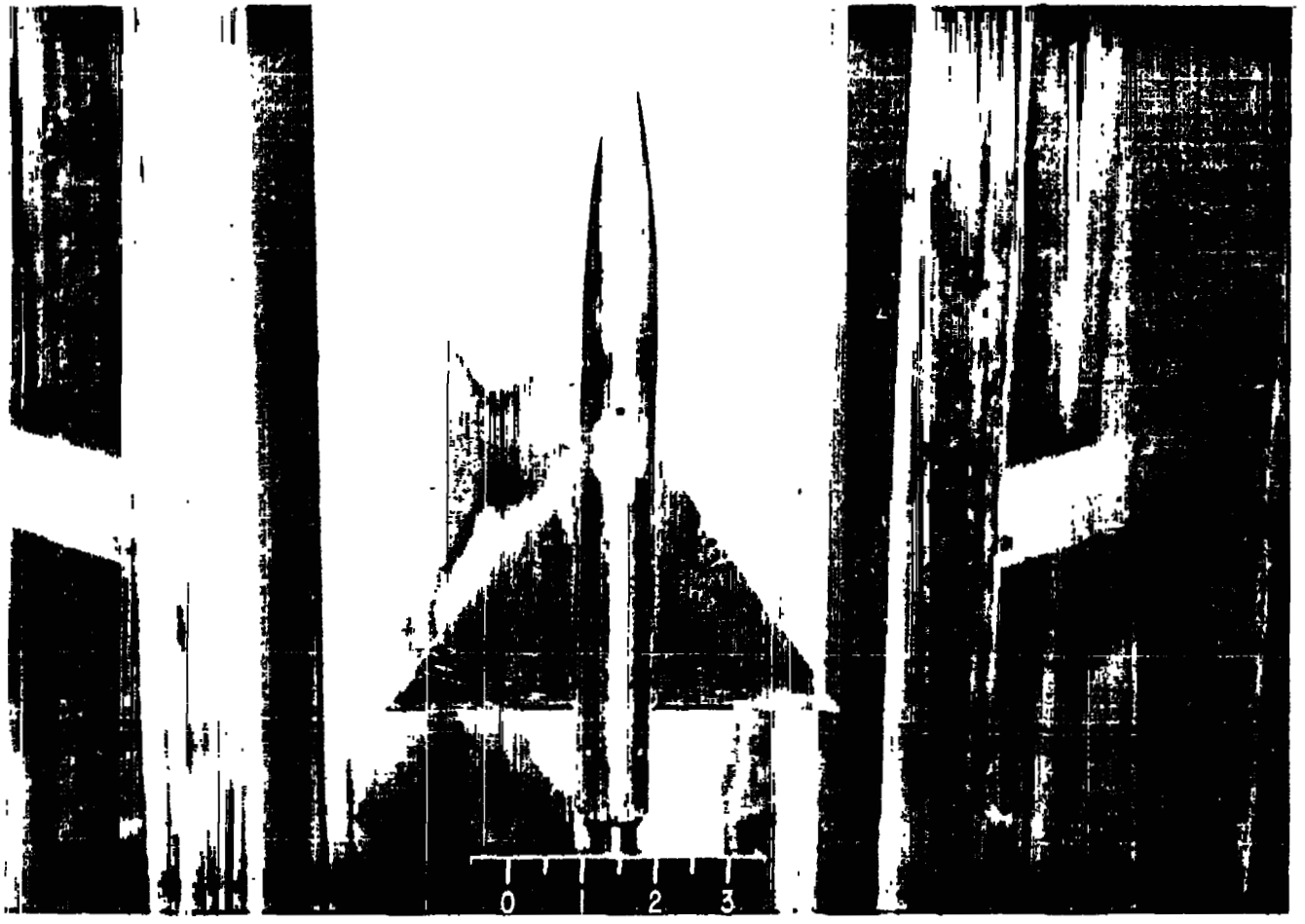

(b) Plan view of the model on the sting. L-82637

Figure 3.- Concluded.

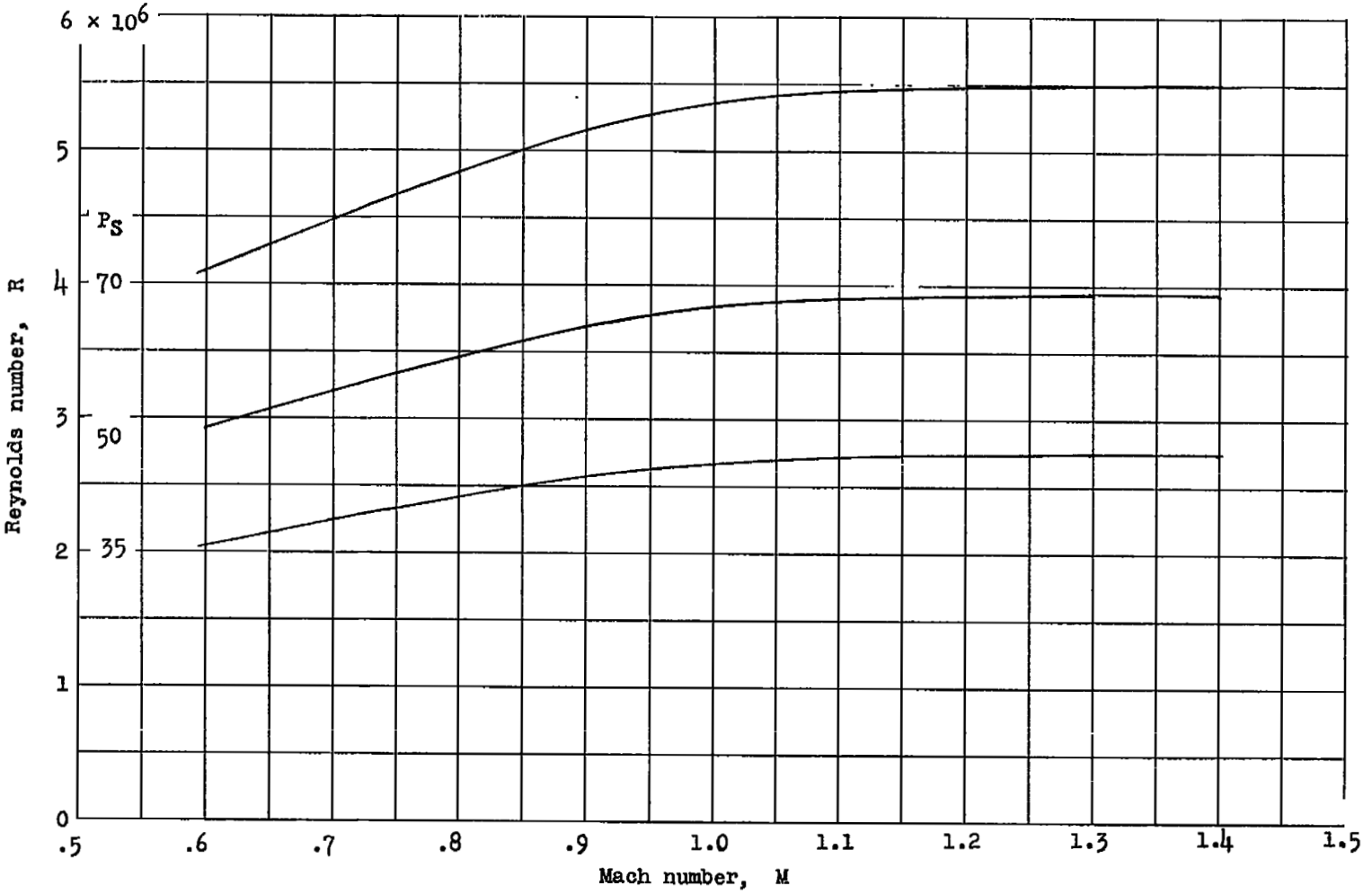

Figure 4.- Variation of Reynolds number with Mach number for stagnation pressures of 35, 50, and 70 pounds per square inch.

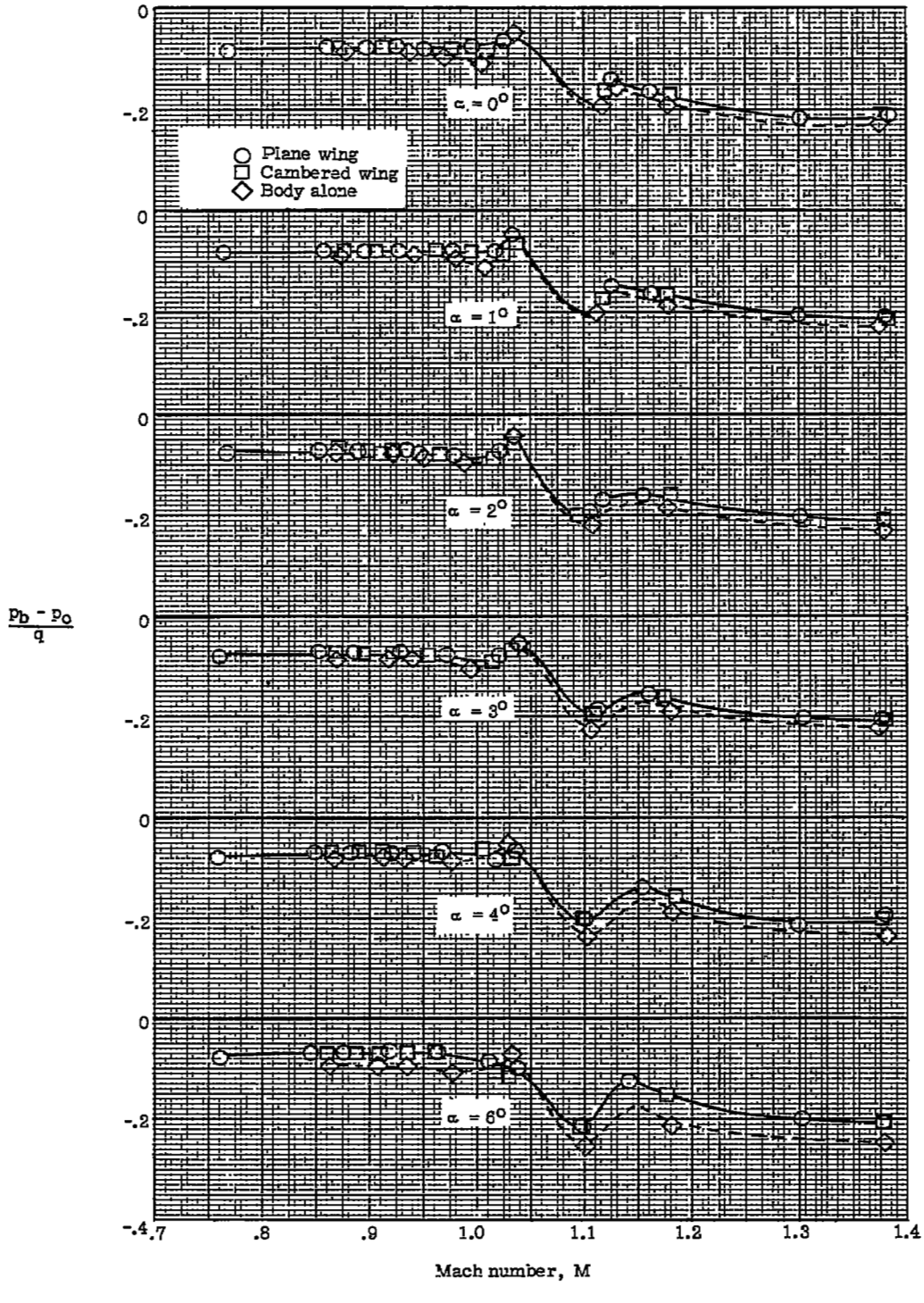

Figure 5.- Variation of base-pressure coefficient with Mach number for each configuration tested.

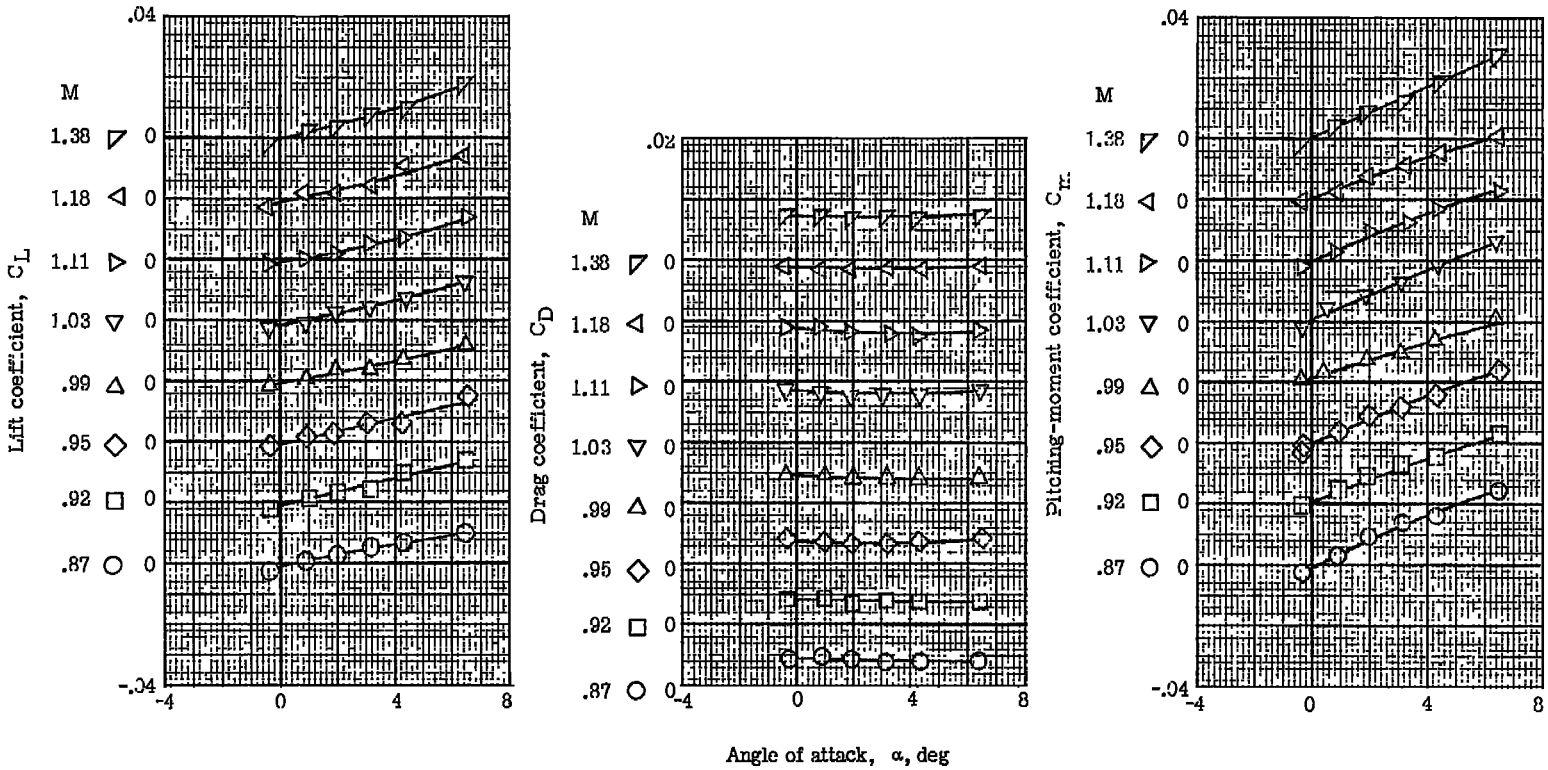

Figure 6.- Variation of lift, drag, and pitching-moment coefficients with angle of attack at various Mach numbers for the body alone.

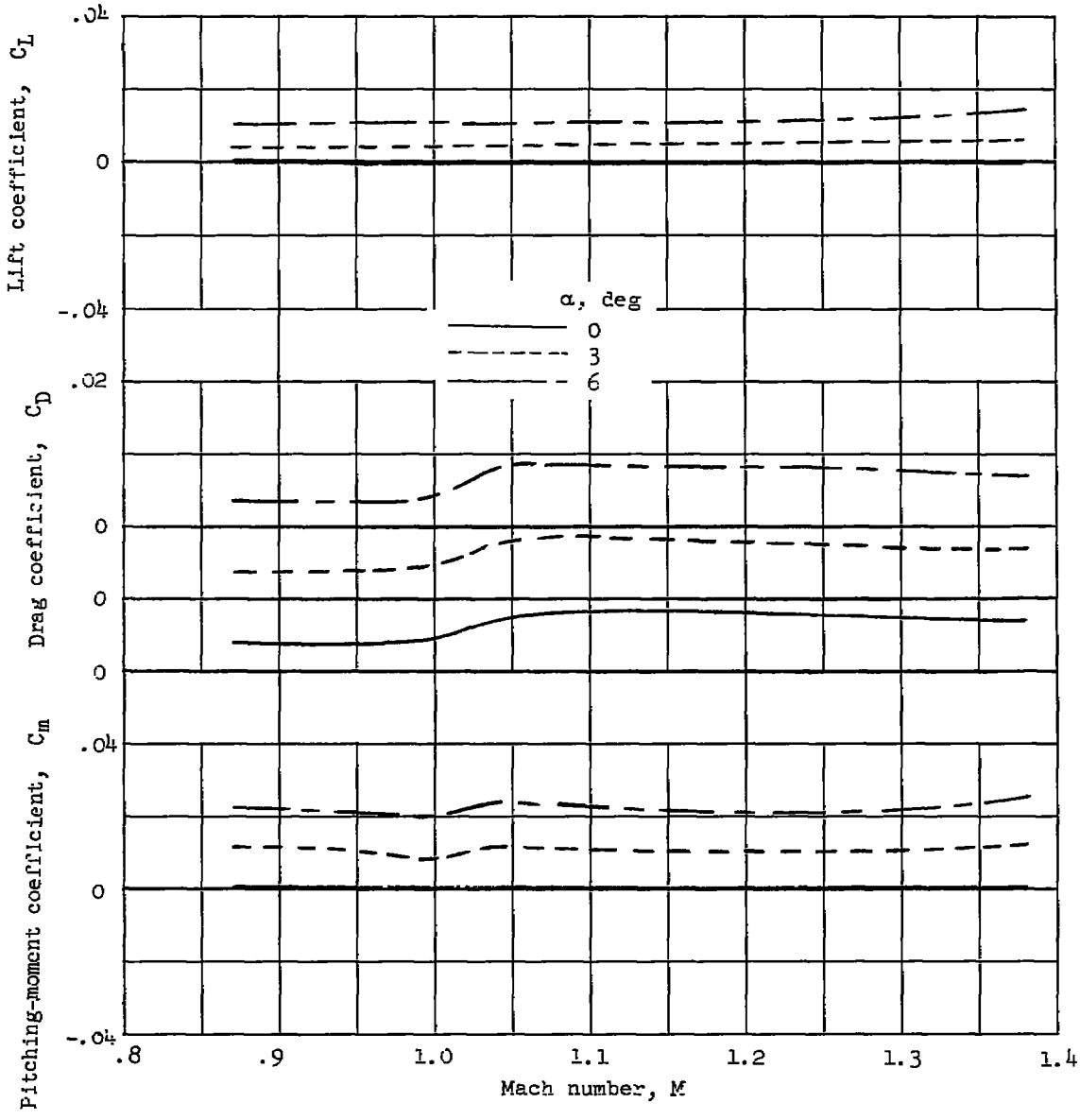

Figure 7.- Variation of lift, drag, and pitching-moment coefficients with Mach number for the body alone. $\alpha = 0^\circ$, 3°, and 6°.

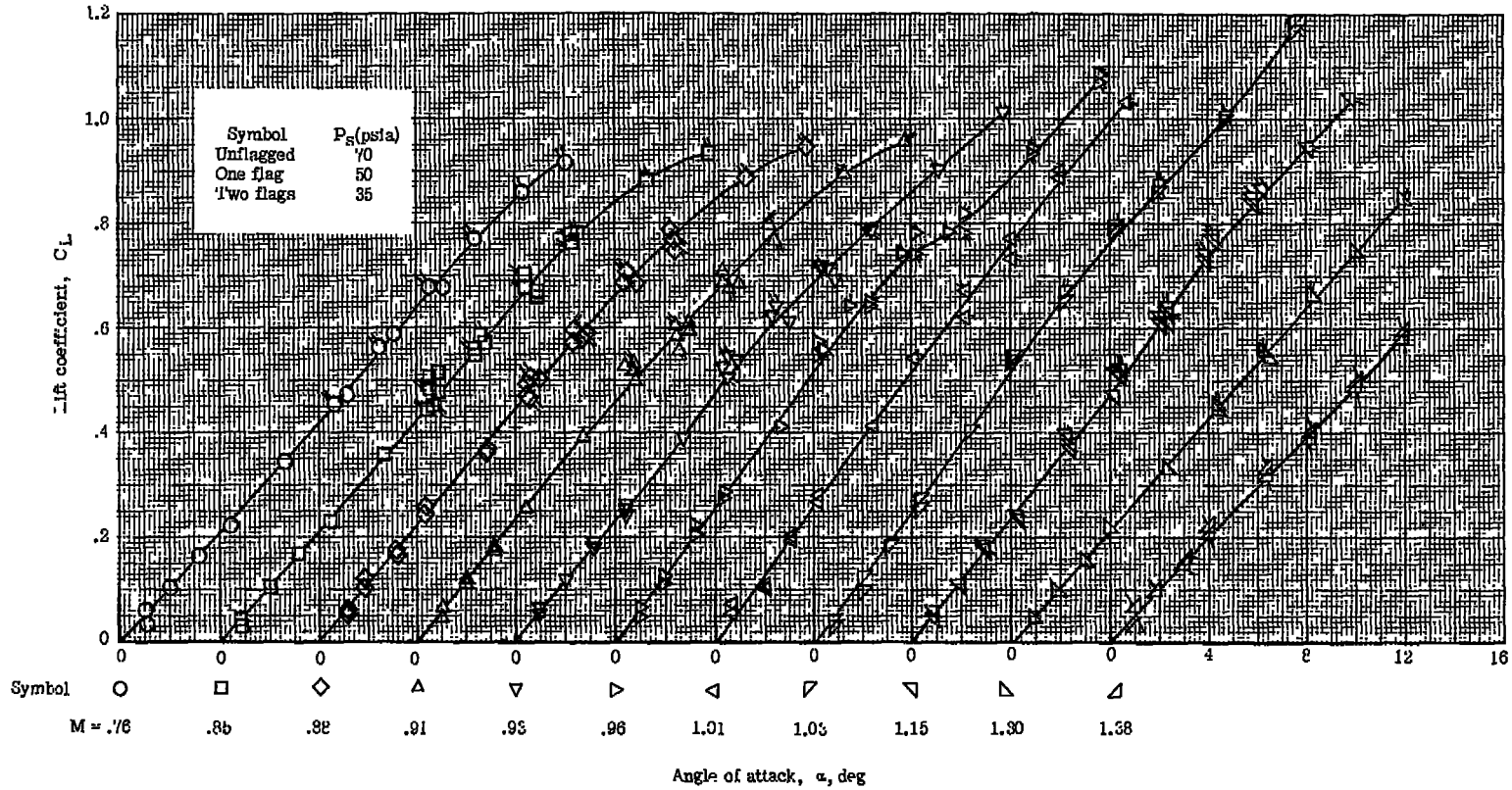

(a) Plane wing.

Figure 8.- The variation of lift coefficient with angle of attack at various Mach numbers.

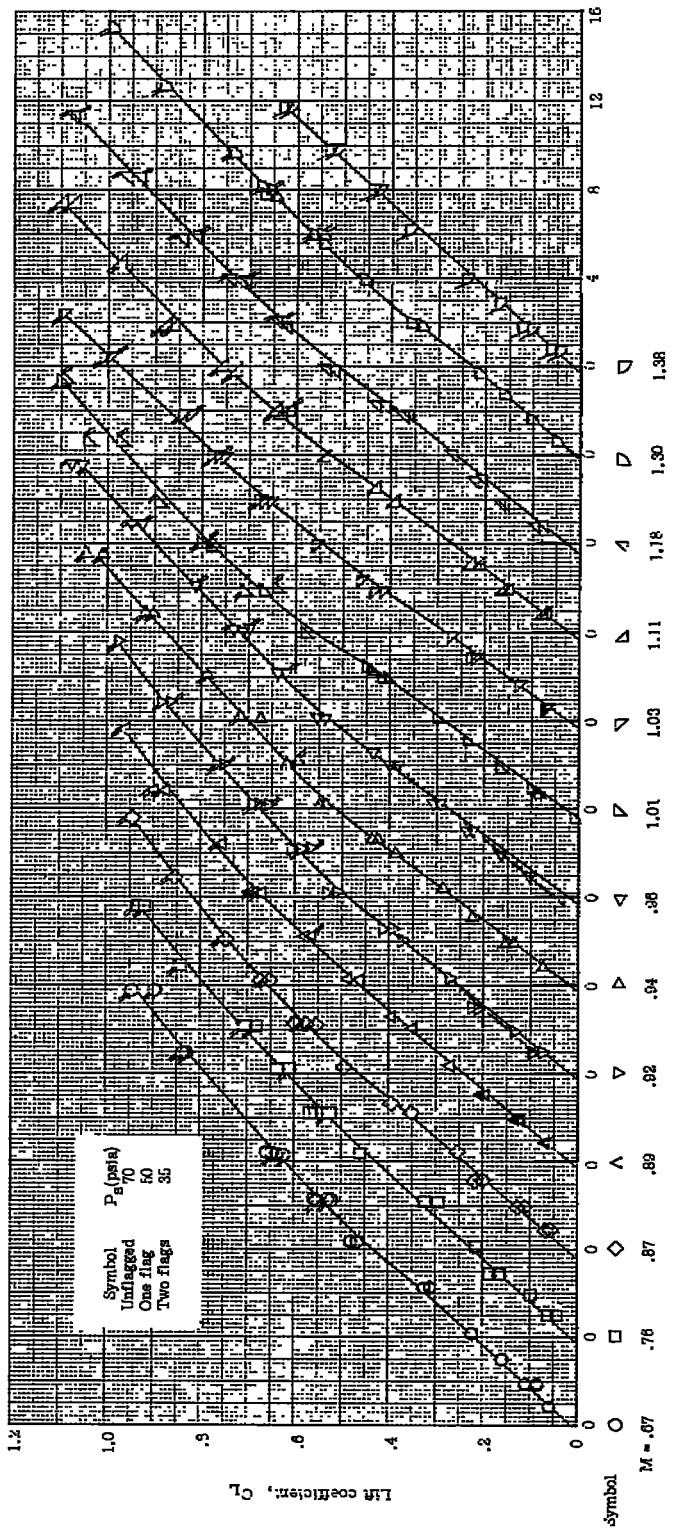

(b) Cambered wing.

Figure 8.- Concluded.

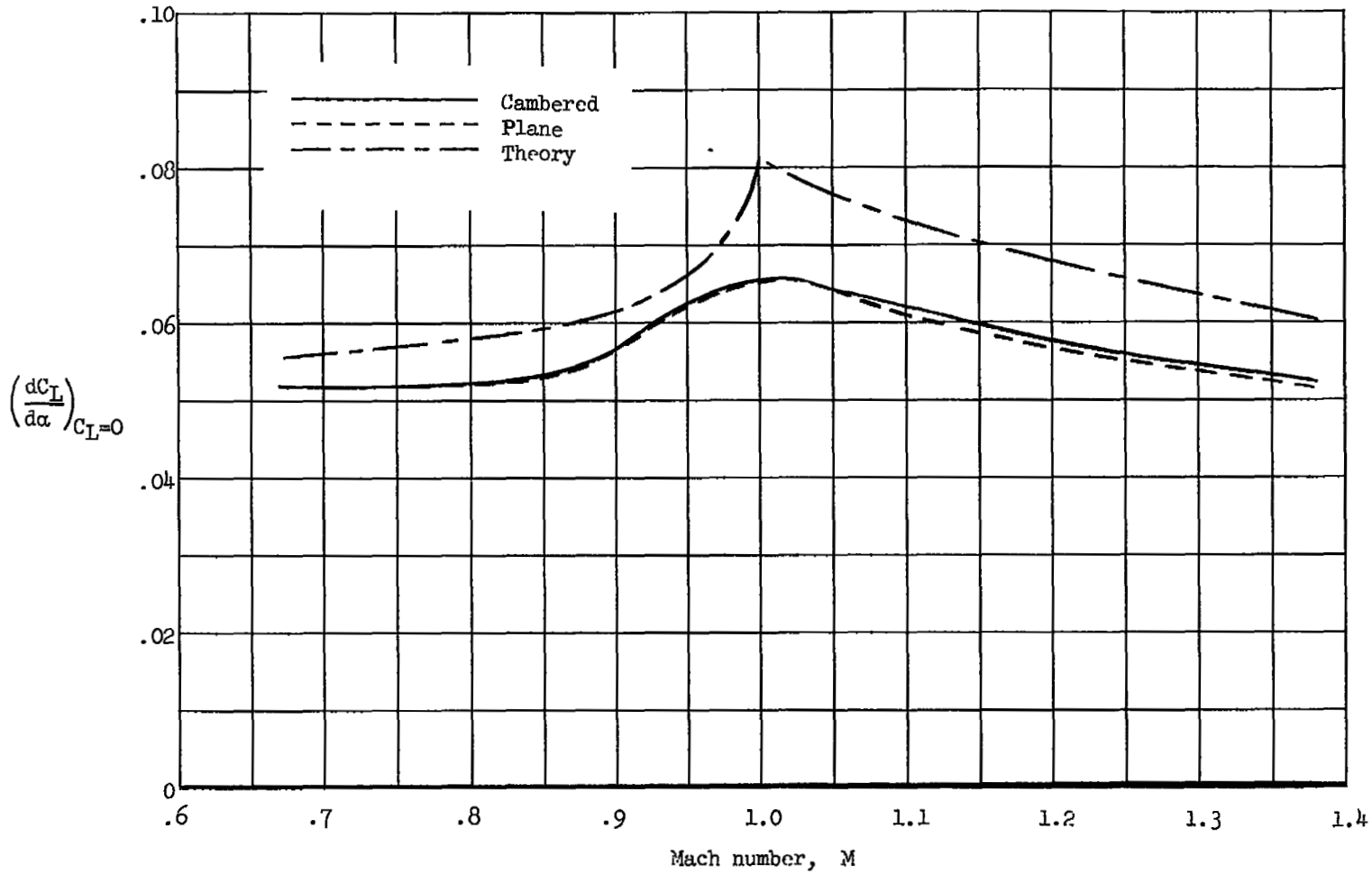

Figure 9.- Variation of lift-curve slope at zero lift with Mach number.

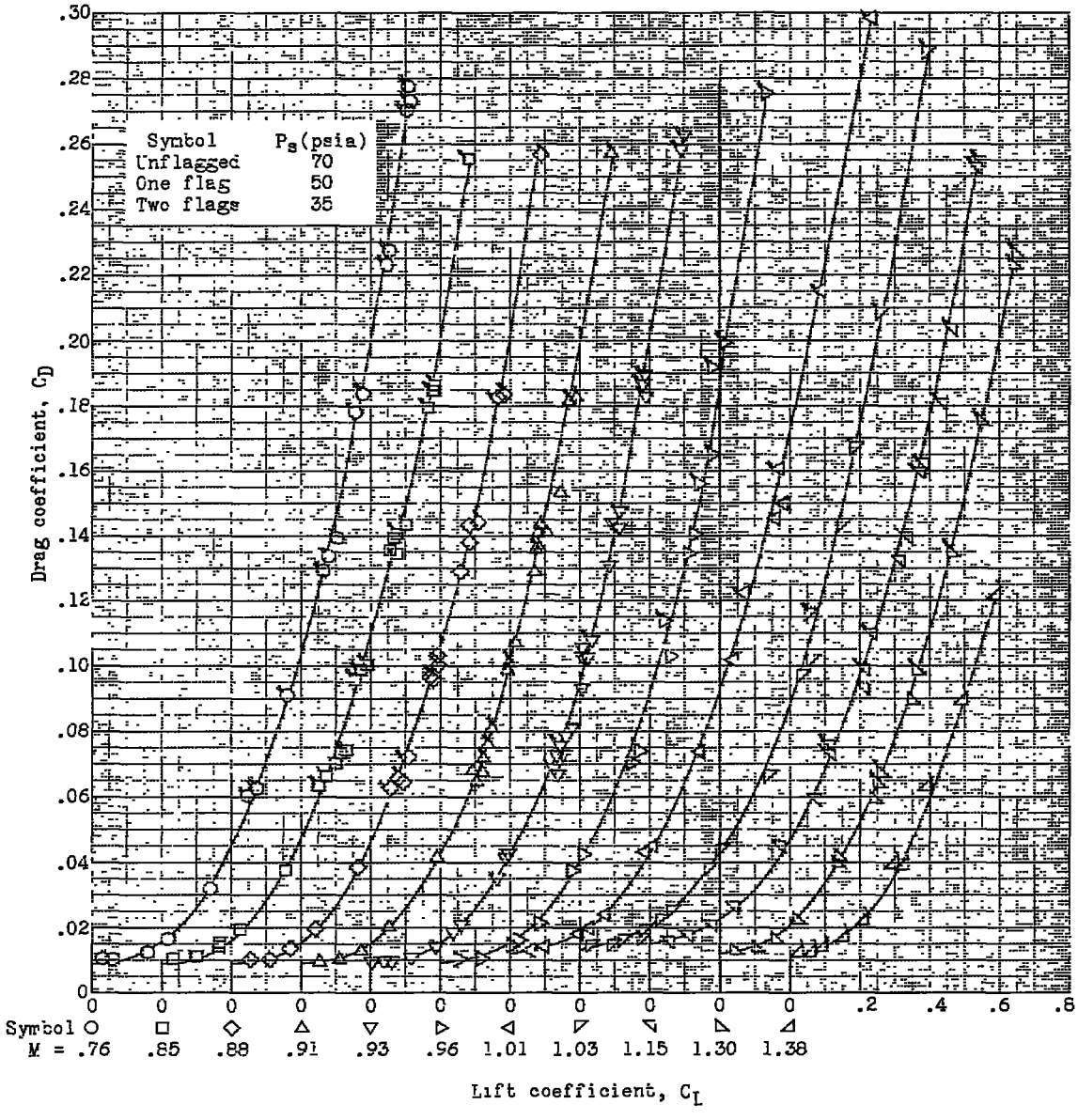

(a) Plane wing.

Figure 10.- Variation of drag coefficient with lift coefficient at various Mach numbers.

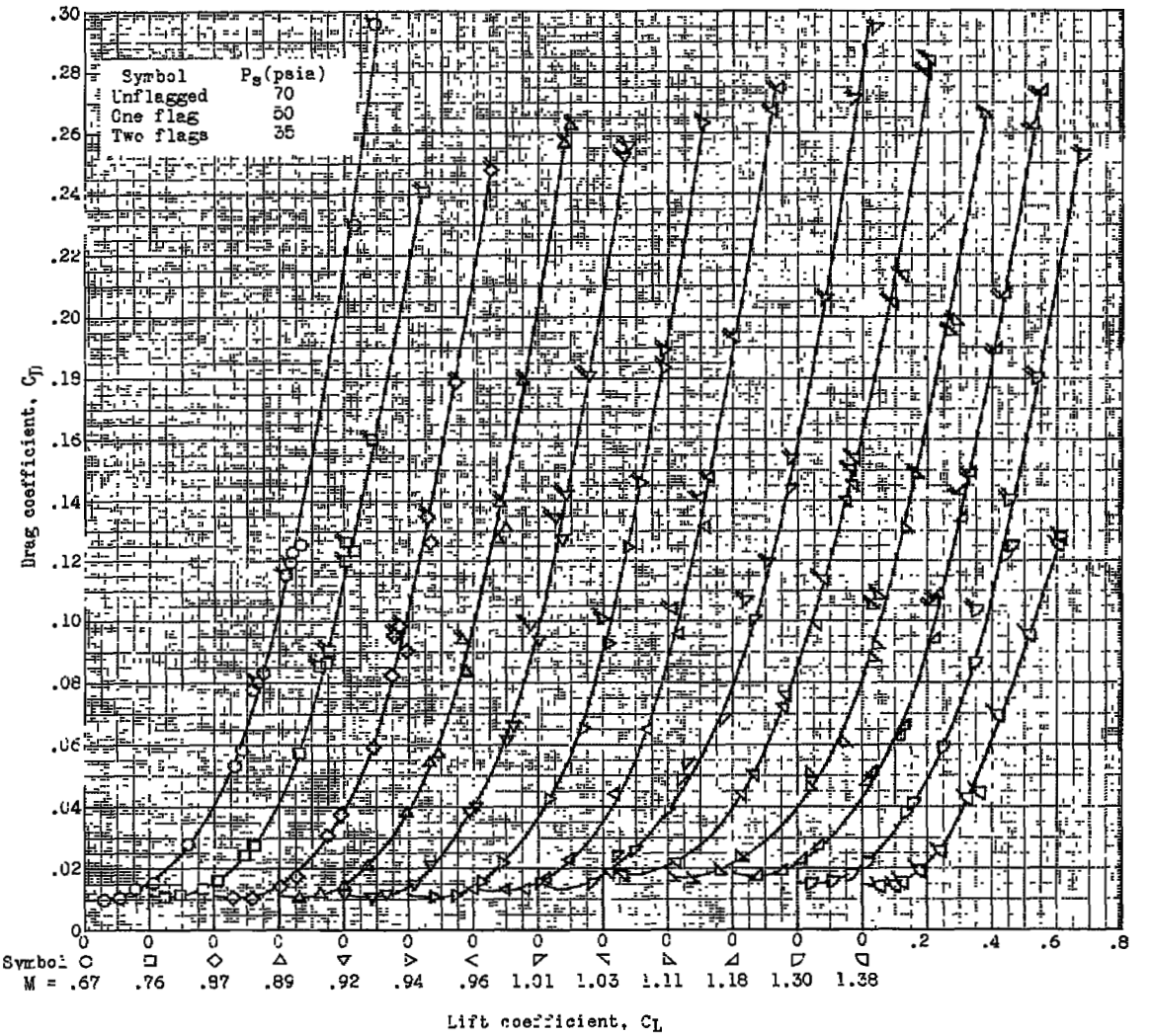

(b) Cambered wing.

Figure 10.- Concluded.

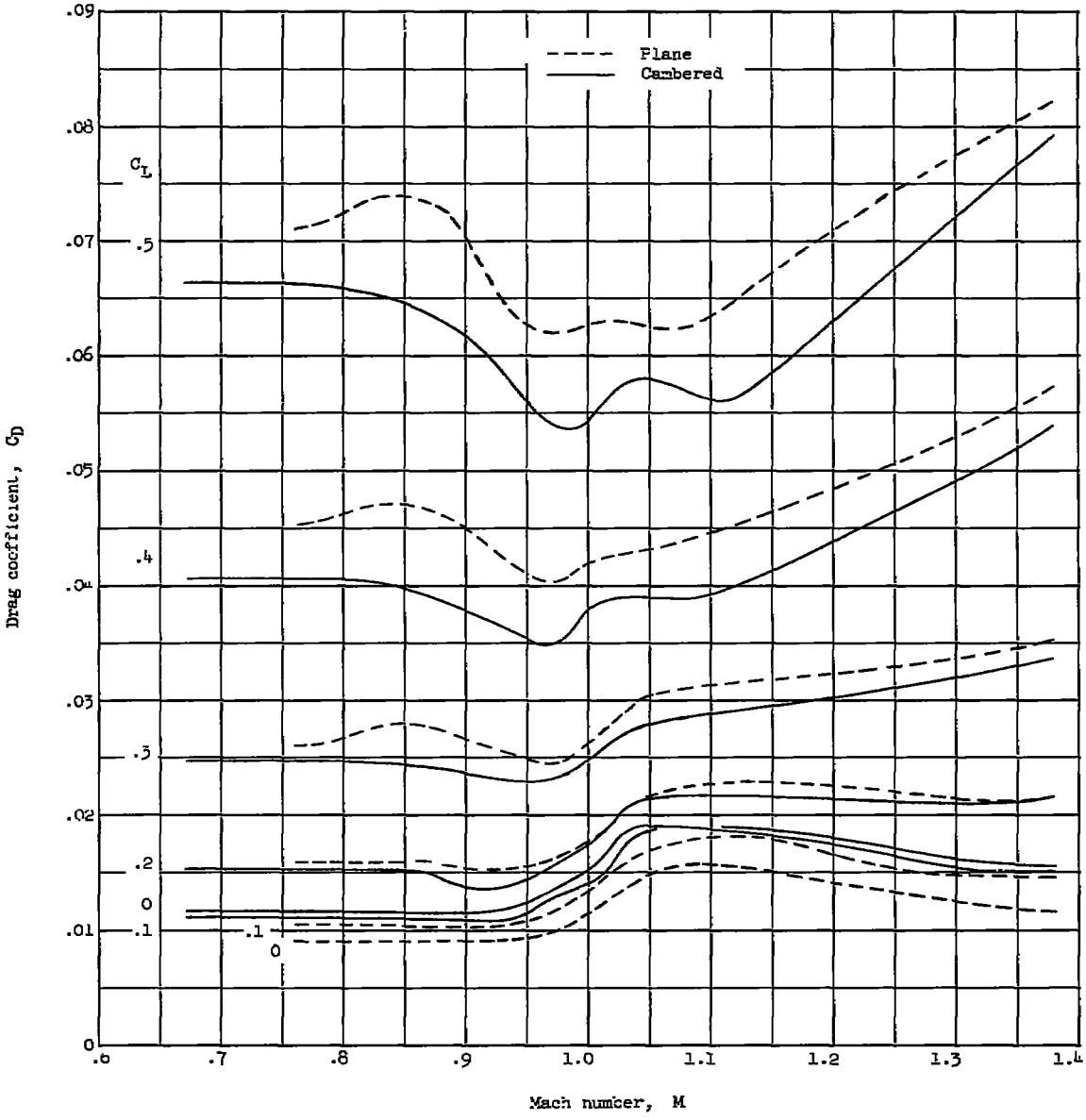

Figure 11.- Variation of drag coefficient with Mach number at various values of lift coefficient.

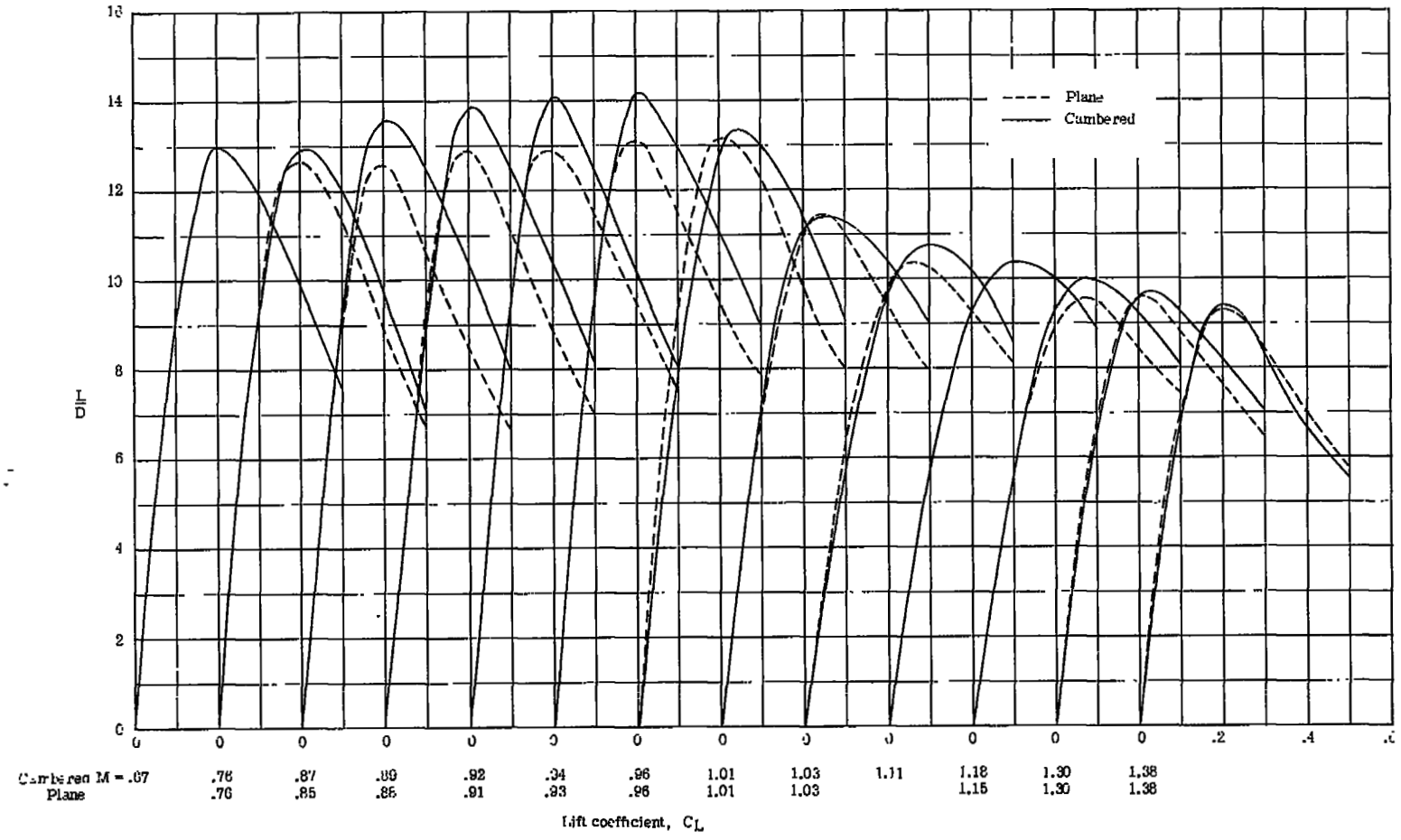

Figure 12.- The variation of lift-drag ratio with lift coefficient at various Mach numbers.

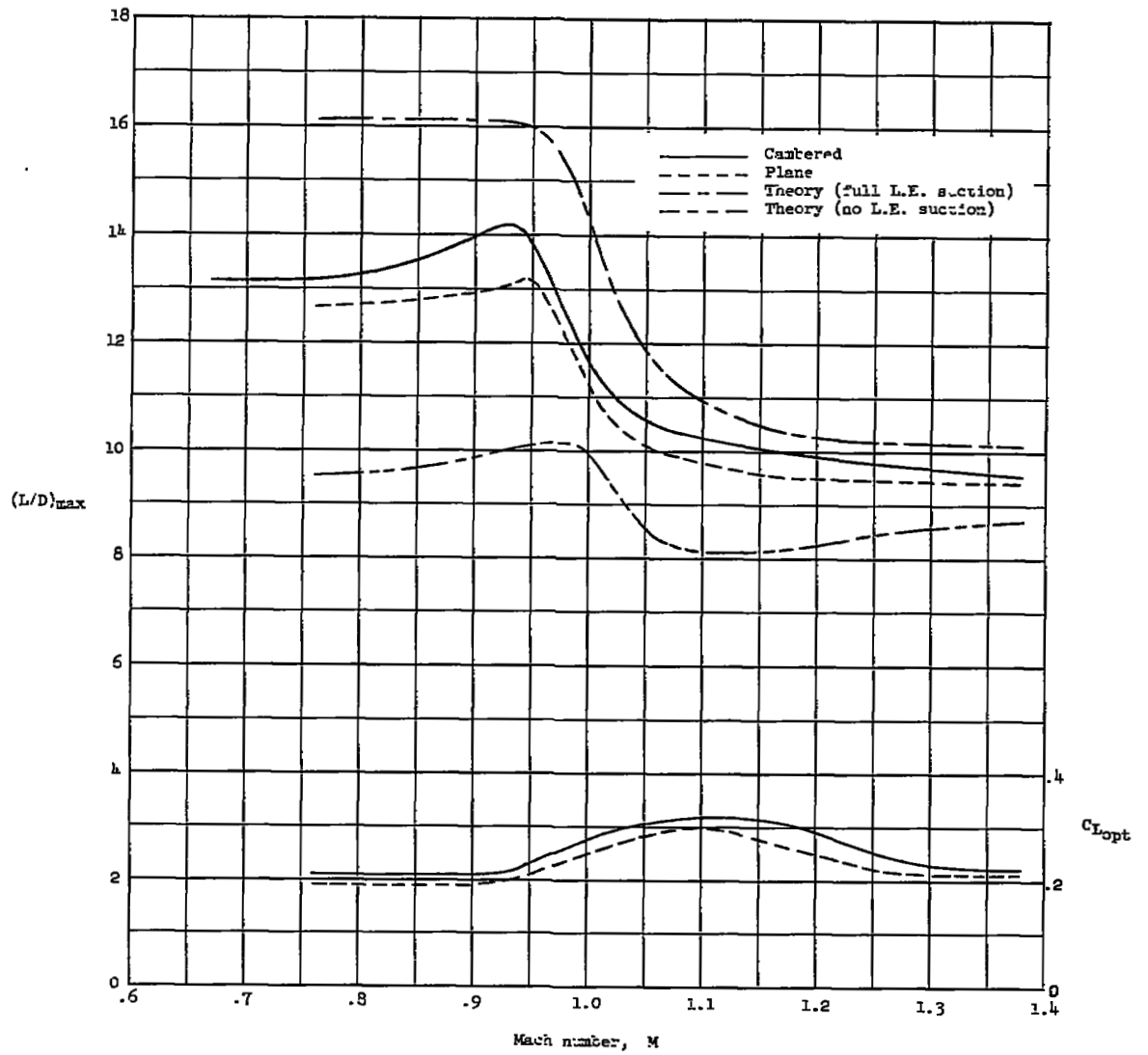

Figure 13.- Variation of $(L/D)_{max}$ and $C_{L_{opt}}$ with Mach number.

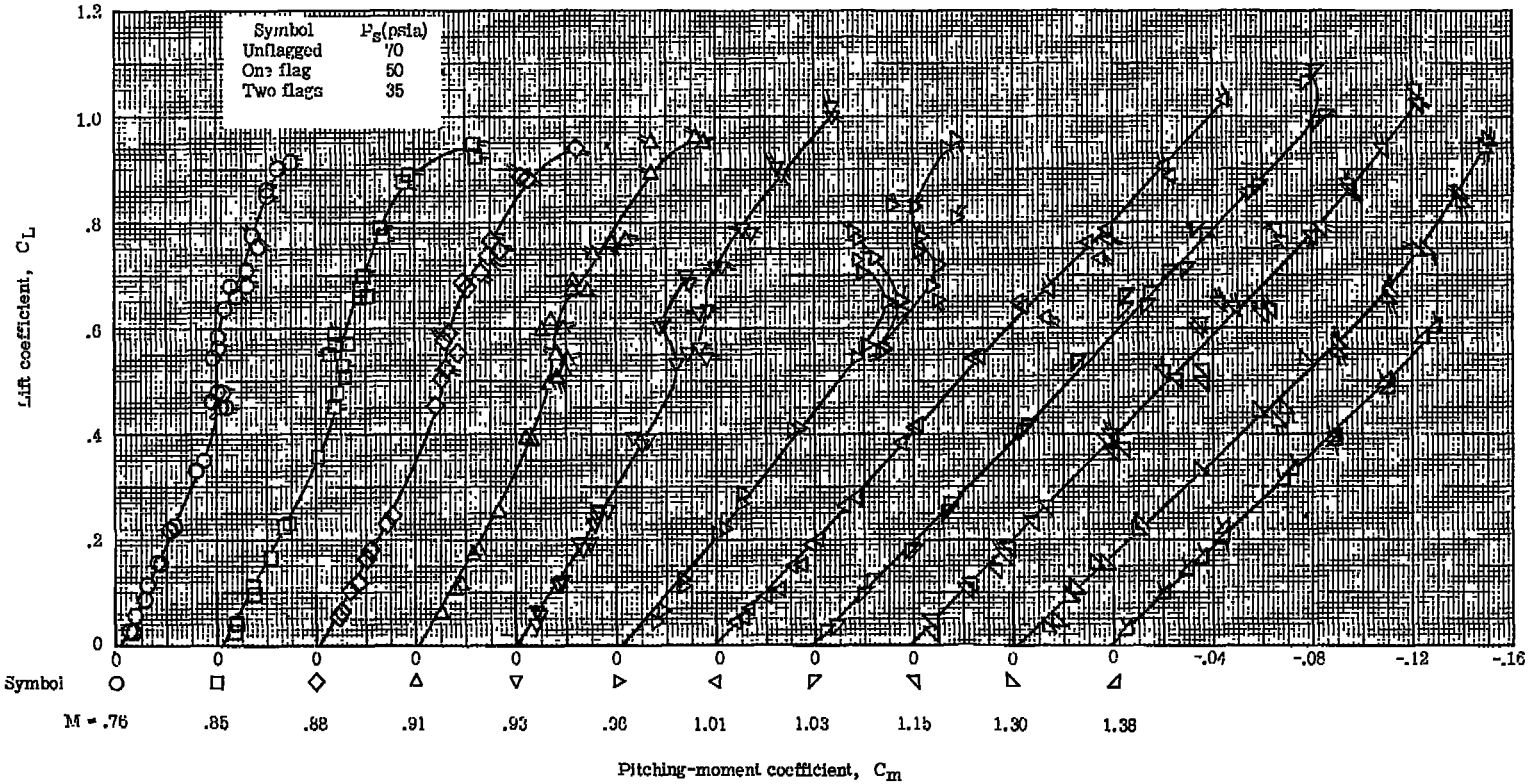

(a) Plane wing.

Figure 14.- Variation of lift coefficient with pitching-moment coefficient at various Mach numbers.

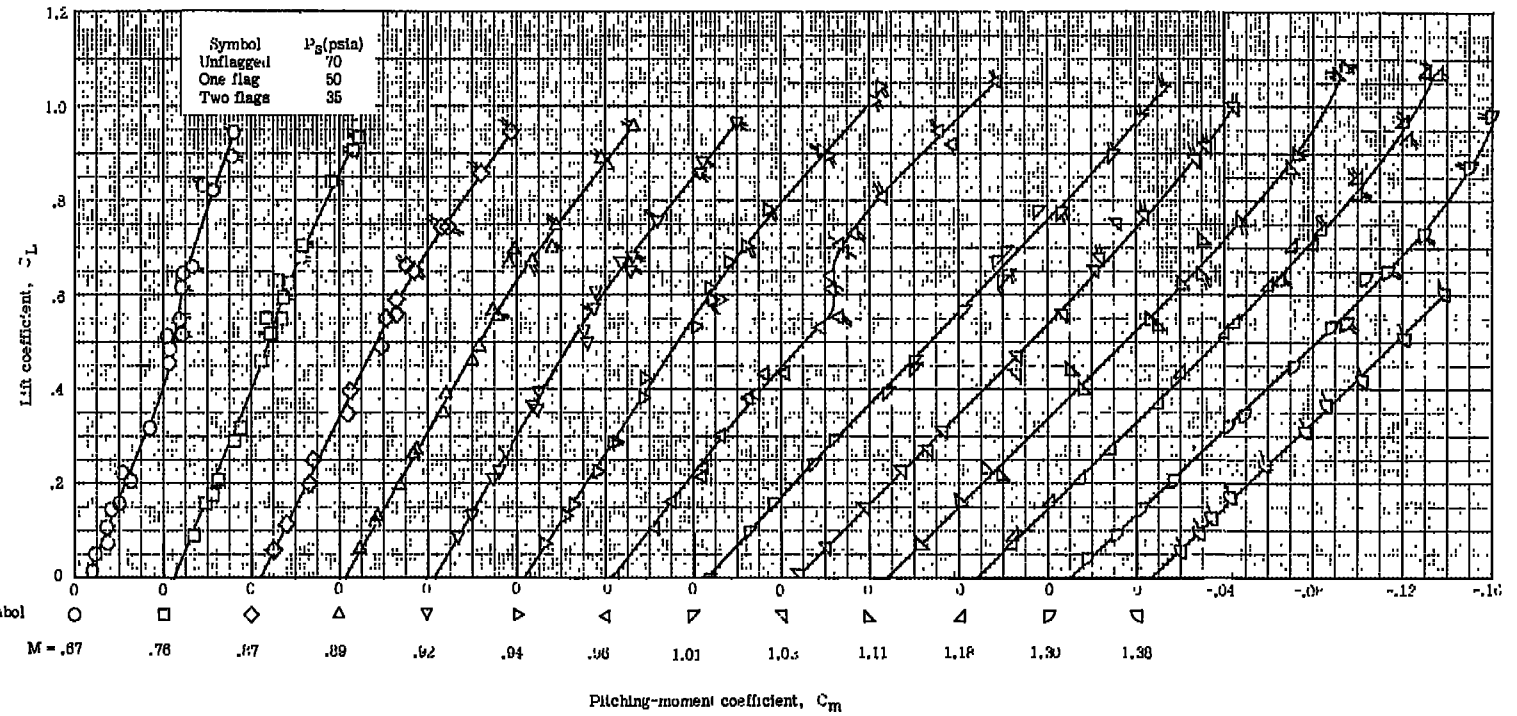

(b) Cambered wing.

Figure 14.- Concluded.

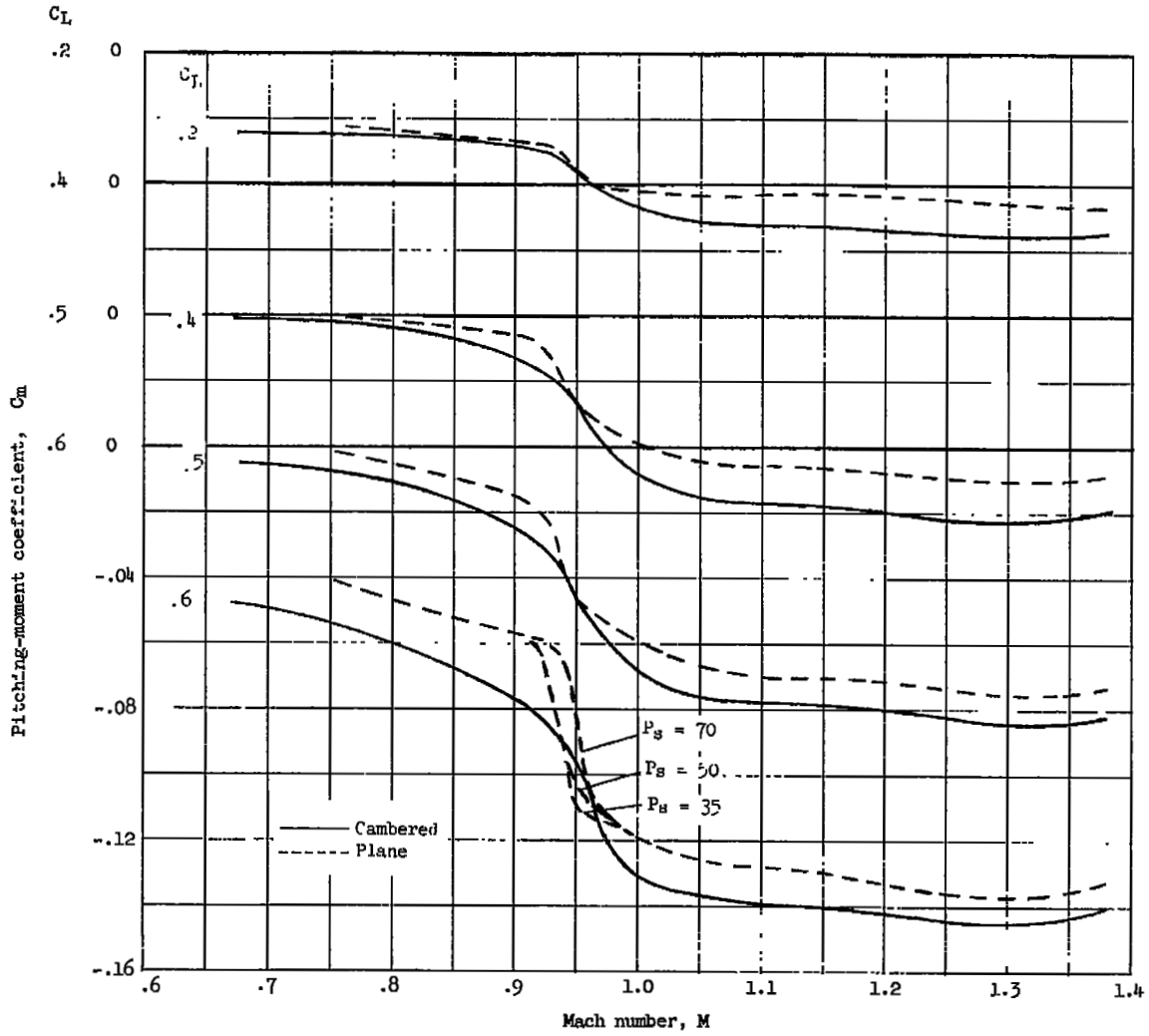

Figure 15.- Variation of pitching-moment coefficient with Mach number at various lift coefficients.

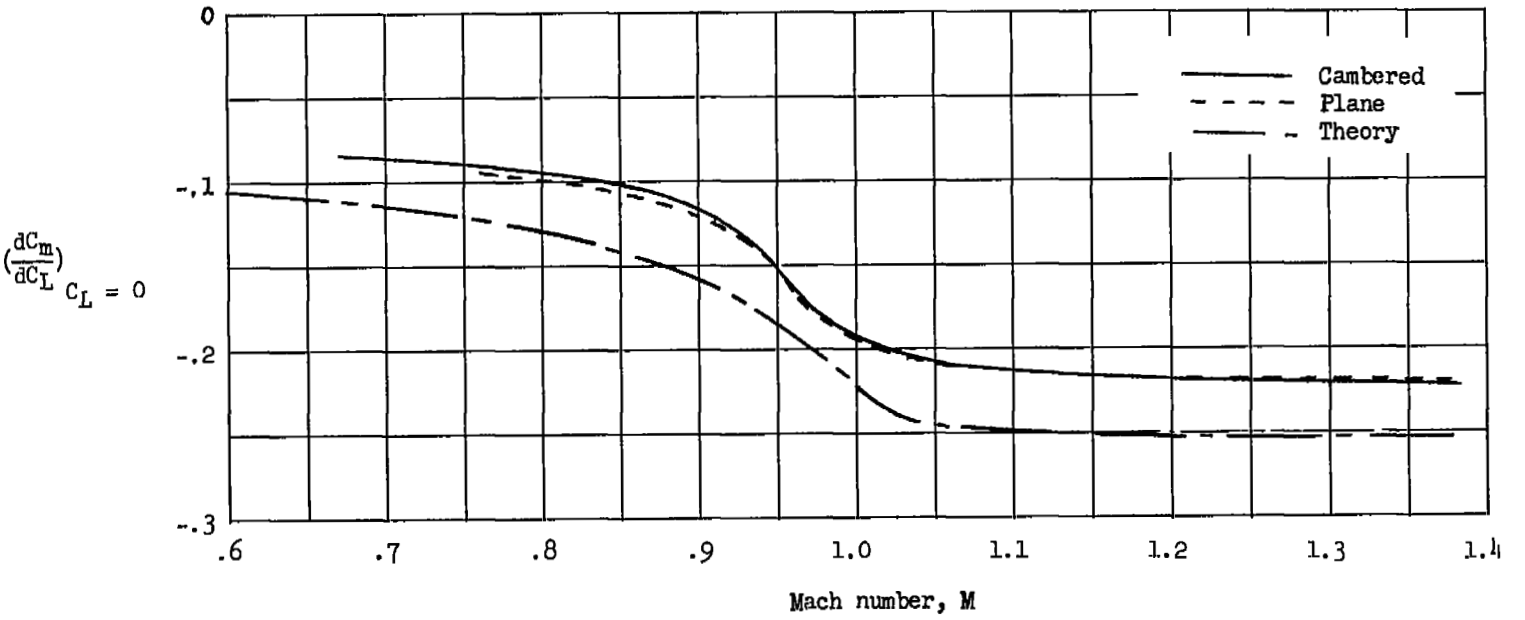

Figure 16.- Variation of pitching-moment-curve slope with Mach number.